The Astrophysical Journal, 703:507–516, 2009 September 20 doi:10.1088/0004-637X/703/1/507

TESTING PULSAR RADIATION MODELS USING AN α-WEAK-DEPENDENT ALTITUDE RATIO

K. J. Lee[1], X. H. Cui[1], H. G. Wang[2], G. J. Qiao[1], and R. X. Xu[1]
[1] Astronomy Department, School of Physics, Peking University, Beijing 100871, China; kjlee007@gmail.com
[2] Center for Astrophysics, Guangzhou University, Guangzhou 510400, China
Received 2008 December 19; accepted 2009 June 26; published 2009 August 28

ABSTRACT

It is found that pulsar radiation altitude ratios between different radio frequencies are weak-dependent on the inclination angle α. This is proved via series expansion techniques and illustrated by using pulsar examples of PSR B0329+54, B1508+55, B2016+28, B1133+16, and B2319+60. It is emphasized that this α-weak-dependent radiation altitude ratio offers a good tool to test pulsar radiation models. We use the measured altitude ratios to constrain the parameter space for the Ruderman–Sutherland model and the inverse Compton scattering model. It is found that the Ruderman–Sutherland model is not compatible with the measured altitude ratios, while the results are compatible with the inverse Compton scattering model. The potential possible applications of this method in studying pulsar timing and in studying pulsar high energy radiation are also discussed.

Key words: dense matter – pulsars: general – stars: neutron

1. INTRODUCTION

Measuring the altitudes of radiation location is of great importance for the research of the pulsar radiation mechanism as well as research for physical processes in a pulsar magnetosphere. At present, there are three kinds of methods to measure the altitudes. The first group of methods uses the information of relative phase shift between pulse components or uses phase shift between polarization features and pulse components (Blaskiewicz et al. 1991; Phillips 1992; Gangadhara & Gupta 2001; Gangadhara 2005; Johnston et al. 2007). The second group of methods uses the geometrical properties of the radiation beam to measure the altitudes (Cordes 1978; Gil & Kijak 1993; Kijak & Gil 1997). The third group of methods uses synthetic information, including geometrical, temporal and spatial information, to calculate the radiation locations (Wang et al. 2006). The inclination angle is a basic parameter in measuring altitude. It can be obtained by fitting the linear polarization position angle curve with a rotating vector model (hereafter RVM; Radhakrishnan & Cooke 1969) or by using some statistical relations (Lyne & Manchester 1988; Rankin 1983). But due to the following two main issues, uncertainty exists in the measured inclination angle of radio pulsars, hence uncertainty is inevitable in the induced absolute emission altitude. (1) The RVM does not work well for pulsars with lower degree of polarization or for pulsars with complex polarization structure (Wang et al. 2006). (2) The statistical relation between the angular width of the radio radiation cone and the period of the pulsar is of large scattering.

Although the uncertainty of the inclination angle (α) will lead to uncertainties when measuring the absolute radiation altitudes of pulsar, we will show that the ratio between two radiation altitudes of two different frequencies are insensitive with respect to the pulsar inclination angle, if the pulsars have steep slopes in linear polarization position angle curves. For such pulsars, the ratio between two radiation altitudes is a better measurable quantity than absolute radiation altitude. This α-weak-dependence ratio validates the measurement of radius-to-frequency mapping (RFM) index, because measuring RFM index, in fact, only involves measuring the ratios between radiation altitudes. We choose five pulsars (PSR B0329+54, B1508+55, B2016+28, B1133+16, and B2319+60) to show such invariance and to illustrate how to use the ratio to test pulsar radiation models, which predict different RFM (Kijak & Gil 2003). Here, the Ruderman–Sutherland model (Ruderman & Sutherland 1975) and the inverse Compton scattering model are examined using altitude ratio.

The Ruderman–Sutherland model (RS model; Ruderman & Sutherland 1975) is a classical radiation model for radio pulsars. In the RS model, an inner vacuum polar magnetospheric gap is formed, where an electric field along the magnetic field lines is produced. The gap continuously breaks down by forming electron–positron pairs. The primary pairs and secondary pairs lead to coherent microwave radiation due to the curvature radiation process. The radiation altitude r for the RS model is $r \propto \omega^{-2/3}$, where ω is the radio wave frequency. We will show in Section 3 that such a RFM of the RS model is incompatible with the altitude ratios of the pulsars we selected. An inverse Compton scattering (ICS) model for radio pulsars has been proposed for nearly 20 years (Qiao 1988; Qiao & Lin 1998; Xu et al. 2000; Qiao et al. 2001). The pulsar radiation beam morphology, radio spectrum, luminosity, and polarization properties of pulsar are explained in the ICS model. Furthermore, the ICS model also predicts the relation between the radiation altitude and the frequency. There are three free parameters in the ICS model, the initial radio wave frequency ω_0, the initial Lorentz factor γ_0, and the energy loss rate ξ. In this paper, we have constrained the parameter space for γ_0 and ξ_0 of the ICS model using the altitude ratios of the pulsar samples.

This paper is organized as follows: in Section 2, the method to measure the ratio between two radiation altitudes is presented; applications for the RS model and the ICS model are given in Section 3; conclusions and discussions are made in Section 4.

2. ACCURATE MEASUREMENT FOR THE RATIO BETWEEN RADIATION ALTITUDES

2.1. Geometrical Method

In this section, the method to calculate the radiation altitudes is described. It is shown why the ratio between two radiation altitudes is nearly invariant with respect to the changing of the inclination angle α, if the slope κ of the linear polarization position angle curve is steep. We adopt notation for geometrical parameters, which are defined in Table 1 and illustrated in Figure 1. More details of deriving the following equations are

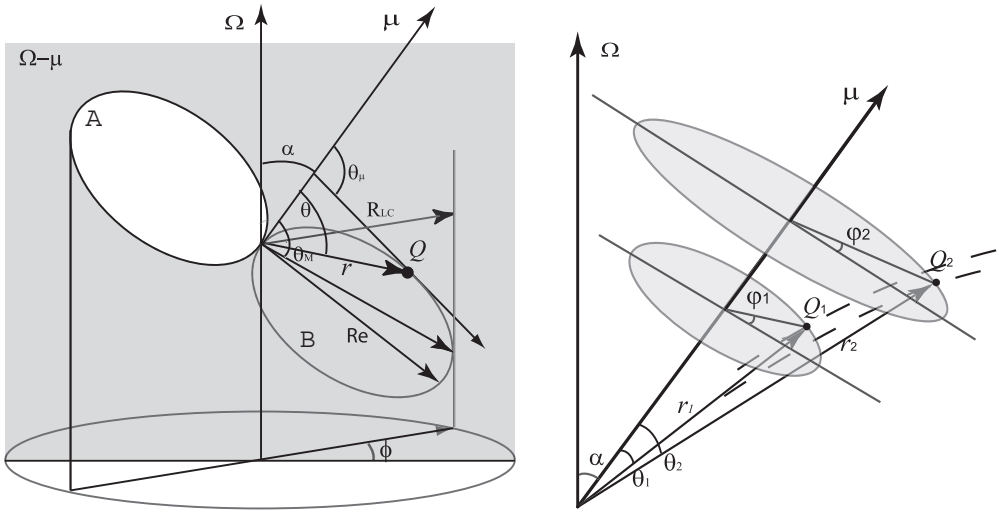

Figure 1. Three-dimensional sketch for the geometrical configuration of the magnetic field line and emission beams. In the left panel, the rectangular gray plane indicates the Ω–μ plane, where Ω and μ are the rotational axis and the magnetic axis, respectively. The magnetic field lines "A" are in front of the Ω–μ plane and magnetic field lines "B" are in the back of the Ω–μ plane. "Q" indicates the radiation source, which is located at altitude r from the pulsar center. θ denotes the polar angle of the radiation source in the magnetic coordinate. θ_μ is the half of the beam angular width. $R_{\rm LC}$ is the radius of the light cylinder for a given magnetic field line, on which the maximal radius is $R_{\rm e}$ from the pulsar center. For an observer, ϕ is the azimuthal angle in the laboratory frame. The right panel shows two radiation beams coming from positions Q_1 and Q_2, respectively. φ is the azimuthal angle in the magnetic coordinate.

Table 1
Symbols Used in Calculation

Symbol	Meaning
p	Period of the pulsar
R	Pulsar radius
ψ	Polarization position angle
ϕ	Azimuthal angle in laboratory frame
θ_μ	Half width of the radiation beam
$\Delta\phi$	Half pulse width of the pulse profile
θ	Polar angle in the magnetic coordinate
φ	Azimuthal angle in the magnetic coordinate
$R_{\rm LC}$	Radius of the light cylinder
$R_{\rm e}$	Maximal radius of a given magnetic field line
$\theta_{\rm M}$	Polar angle in the magnetic coordinate for the light tangential point of the magnetic line to cylinder
η	Ratio between two polar angles of radiation sources
$\overline{\eta}$	Average of η
ζ	Ratio between two altitudes of radiation sources
$\overline{\zeta}$	Average of ζ
c	Light speed
α	Inclination angle
β	Impact angle, the angle between the line of sight and the magnetic axis

given in the Appendix. The basic assumptions used throughout the paper are as follows. (1) The pulsar magnetic field is dipolar. (2) The radio emission directions are parallel to the local magnetic field. (3) The RVM is applicable to calculate the maximal slope of the linear polarization position angle curve.

The maximal slope κ of the linear polarization position angle curve can be measured from the radio polarization data (Radhakrishnan & Cooke 1969; Lyne & Manchester 1988). This maximal slope κ gives a relation between the inclination angle α and the impact angle β (Lyne & Manchester 1988) as

$$\kappa \equiv \left.\frac{d\psi}{d\phi}\right|_{\rm max} = \frac{\sin\alpha}{\sin\beta}. \quad (1)$$

Given α and β, assuming that the radiation beam is symmetric with respect to the magnetic axis, the half angular beam width θ_μ relates to $\Delta\phi$ by Gil et al. (1984) and Lyne & Manchester (1988):

$$\sin^2\left(\frac{\theta_\mu}{2}\right) = \sin^2\left(\frac{\Delta\phi}{2}\right)\sin\alpha\,\sin(\alpha+\beta) + \sin^2\left(\frac{\beta}{2}\right), \quad (2)$$

where $2\Delta\phi$ is the total pulse width measured at a 10% pulse amplitude level (see Equation (22) for details).

Assuming the dipole magnetic field configuration, the radiation coming from the location with magnetic polar angle θ forms the radiation beam with half angular beam width of θ_μ given (Qiao et al. 2001)

$$\tan\theta_\mu = \frac{3\sin 2\theta}{1+3\cos 2\theta} \quad (3)$$

or inversely

$$\theta = \frac{1}{2}\arccos\left[\frac{\sqrt{\sin^4\theta_\mu - 10\sin^2\theta_\mu + 9} - \sin^2\theta_\mu}{3}\right]. \quad (4)$$

The radiation beam is observed by an observer with viewing angle $\alpha+\beta$, then the azimuth angle of the boundary field line reads

$$\varphi = \arccos\left[\frac{\cos\alpha\cos\theta_\mu - \cos(\alpha+\beta)}{\sin\alpha\sin\theta_\mu}\right], \quad (5)$$

where φ is defined in the magnetic polar coordinate.

Now we have complete angular information about where the radiation comes from, which is given by the angular coordinates $\{\theta, \varphi\}$. The θ denotes the polar angle of radiation location, while the φ denotes the azimuthal angle of radiation location in the magnetic polar coordinate. We now turn to calculate the radiation altitude. In the dipolar field approximation, the radiation altitude is $r = R_{\rm e}\sin^2\theta$, where $R_{\rm e}$ can be calculated for a field line with ϕ by the following equation:

$$R_{\rm e} = \frac{R_{\rm LC}}{\sin^2\theta_{\rm M}\sqrt{1-(\cos\alpha\cos\theta_{\rm M} - \sin\alpha\sin\theta_{\rm M}\cos\varphi)^2}}, \quad (6)$$

Table 2
Adopted Parameters for PSR B0329+54, B1508+55, B2016+28, B1133+16, and B2319+60

PSR	Period (s)	κ	$2\Delta\phi_{0.408\,\mathrm{GHz}}$ (deg)	$2\Delta\phi_{1.4\,\mathrm{GHz}}$ (deg)	$2\Delta\phi_{4.8\,\mathrm{GHz}}$ (deg)
PSR B0329+54	0.715	−10.0	28.82 ± 0.06	28.3 ± 0.2	25.17 ± 0.03
PSR B1508+55	0.740	−28.0	14.57 ± 0.3	14.47 ± 0.05	10.1 ± 0.4
PSR B2016+28	0.558	6.0	14.65 ± 0.02	16.31 ± 0.05	15.1 ± 0.1
PSR B1133+16	1.188	12.0	13.20 ± 0.05	12.00 ± 0.03	9.64 ± 0.03
PSR B2319+60	0.717	9.0	24.83 ± 0.3	21.6 ± 0.2	19.60 ± 0.05

Notes. The periods and κ come from Lyne & Manchester (1988). The error of κ is assumed to be 10% throughout the paper, as the original data did not include the discussion of error (Lyne & Manchester 1988). The $2\Delta\phi_{0.408\,\mathrm{GHz}}$, $2\Delta\phi_{1.4\,\mathrm{GHz}}$, and $2\Delta\phi_{4.8\,\mathrm{GHz}}$ are the pulse widths corresponding to 408 MHz, 1408 MHz, and 4850 MHz observation for PSR B0329+54, B2016+28, B1133+16, and B2319+60. For PSR B1508+55, the 4.8 GHz data correspond to 4750 MHz observation. All these widths are measured down to a 10% intensity level by Gaussian fitting. The unit for the width is degree. The pulse profile data are from EPN pulsar database. For PSR B1508+55, the 4750 MHz data are from Seiradakis et al. (1995), all the other data at 4.85 GHz are from von Hoensbroech & Xilouris (1997). The other data are from Gould & Lyne (1998).

in which $R_{\mathrm{LC}} = pc/2\pi$ is the radius of a light cylinder for a pulsar with period p, c is the light velocity, θ_{M} is the magnetic polar angle between the magnetic axis and the tangent point of the magnetic field line to the light cylinder as shown in Figure 1. θ_{M} satisfies

$$\begin{aligned} &2\cos\theta_{\mathrm{M}}(\cos\theta_{\mathrm{M}}\sin\alpha+\cos\alpha\cos\varphi\sin\theta_{\mathrm{M}})^2 \\ &+\sin\theta_{\mathrm{M}}(\cos\alpha\cos\theta_{\mathrm{M}}\cos\varphi-\sin\alpha\sin\theta_{\mathrm{M}})(\cos\theta_{\mathrm{M}}\sin\alpha \\ &+\cos\alpha\cos\varphi\sin\theta_{\mathrm{M}})+3\cos\theta_{\mathrm{M}}\sin^2\theta_{\mathrm{M}}\sin^2\varphi \\ &=0. \end{aligned} \tag{7}$$

Note that there exists only one real solution for θ_{M} between 0 and π, the equation can be readily solved using numerical methods, such as bisect or Newton's step-down methods.

Here is a summary of steps to calculate the radiation altitude ratios.

1. Measure the half pulse width $\Delta\phi$ from pulse profile and find the maximal slope of the linear polarization position angle curve from polarization data.
2. For any given inclination angle α, derive half width θ_μ of the radiation beam from Equations (1) and (2).
3. Substitute θ_μ into Equations (4) and (5), and calculate the angular coordinates $\{\theta, \varphi\}$ for the radiation location.
4. Calculate R_{e} with Equations (6) and (7).
5. Use $r = R_{\mathrm{e}}\sin^2\theta$ to calculate the radiation altitude r.
6. Repeat the above five steps for all the observational frequencies. Once the altitudes at multiple frequencies are figured out, calculate the ratio between radiation altitudes. Define $\eta = \theta_1/\theta_2$ and $\zeta = r_1/r_2$, which are the ratios between the polar angles and between the altitudes of radiation locations at two frequencies, respectively.

To see why the ratio between different altitudes is insensitive to the inclination angle α, we adopt the Taylor expansion technique to investigate the behavior of the altitude ratio when κ is large, i.e., the maximal slope of the linear polarization position curve is steep. Substituting Equation (1) into Equation (2) and carrying out Taylor expansion of θ_μ[3] in terms of α, we have

$$\theta_\mu = A_1\alpha + A_3\alpha^3 + O(\alpha^5), \tag{8}$$

where the coefficients A_1 and A_3 are

$$A_1 = \sqrt{\frac{2\kappa(\kappa+1)-2\kappa\cos(\Delta\phi)(\kappa+1)+1}{\kappa^2}}, \tag{9}$$

$$A_3 = \frac{2\kappa\cos(\Delta\phi)+(\kappa+1)(-\kappa+(\kappa+1)\cos(2\Delta\phi)-3)}{8\kappa^2 A_1}. \tag{10}$$

From Equation (8), we can calculate the ratio between θ_μ at two frequencies as

$$\frac{\theta'_\mu}{\theta_\mu} = \frac{A'_1\alpha + A'_3\alpha^3 + O(\alpha^5)}{A_1\alpha + A_3\alpha^3 + O(\alpha^5)} = \frac{A'_1}{A_1}\left[1+\left(\frac{A'_3}{A'_1}-\frac{A_3}{A_1}\right)\alpha^2 + O(\alpha^4)\right]. \tag{11}$$

As shown by the right side of the above equation, the dependence on α is canceled for the leading term. Because $|A'_3/A'_1 - A_3/A_1| \leqslant |A'_3/A'_1| + |A_3/A_1|$, the smaller the A_3/A_1 is, the lesser the higher order terms would affect (i.e., the coefficients for the α^2 term will be smaller in Equation (11)), which means that the effects of α will be smaller. To make this point clear, the contour map for A_3/A_1 versus κ and $\Delta\Phi$ is plotted in Figure 2, which shows that the A_3/A_1 will be small when κ is large. In this way, our method is valid to determine the radiation altitude ratio to high accuracy for pulsars with a steep slope of the linear polarization position curve. With further simplification, we can use the following formula to estimate the ratio of θ_μ up to the third order, if $\kappa \gg 1$:

$$\frac{\theta_{\mu 2}}{\theta_{\mu 1}} = \sqrt{\frac{1-\cos\Delta\phi_1}{1-\cos\Delta\phi_2}} + \frac{\cos\Delta\phi_1 - \cos\Delta\phi_2}{4\kappa^2\sqrt{1-\cos\Delta\phi_1}(1-\cos\Delta\phi_2)^{\frac{3}{2}}} + O\left(\frac{1}{\kappa^3}\right). \tag{12}$$

Similar check can be performed for ζ by Taylor expansion techniques with the expansion series of r,

$$r = B_2\alpha^2 + B_4\alpha^4 + O(\alpha^6), \tag{13}$$

where

$$B_2 = \frac{4}{9}A_1^2, \tag{14}$$

[3] Because θ_μ and θ have very good semilinear relation $\theta_\mu = 3\theta/2 + \theta^3/8 + O(\theta^5)$, which is derived from Equation (3), the invariance for the ratio of θ_μ leads to invariance for ratio of θ. To simplify the discussion, we show the invariance for ratio of θ_μ instead of θ.

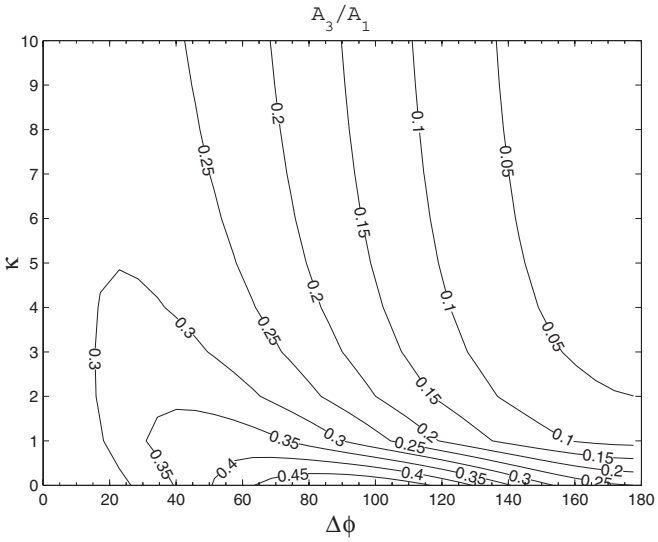

Figure 2. Contour plot for the absolute value of A_3/A_1 in terms of κ and $\Delta\phi$. We can clearly see that the A_3/A_1 is smaller, if the κ is larger. For such a situation, we will have the invariant properties for the ratio (η and ζ) between radiation altitudes with respect to the nclination angle α.

$$B_4 = \frac{\left(144A_1A_3 - 11A_1^4\right)\kappa^4 - 20A_1^2\kappa^3 - 10\left(A_1^2 - 2\right)\kappa^2 + 20\kappa + 5}{162\kappa^4}. \quad (15)$$

Although the expansion technique can show weakly α-dependent behavior of ζ, we prefer to use the ζ–α and η–α plots, like Figures 3–7, to directly check such weak dependence. In Section 3, we have done such check for all the pulsar examples.

We now turn to study how much error for η and ζ is introduced from the observational errors of $\Delta\phi$ and the error of κ. Denoting the errors of $\Delta\phi$ and κ by $\delta\Delta\phi$ and $\delta\kappa$, respectively, the estimation of error for the η is

$$\delta\eta \simeq \sqrt{\left(\frac{\delta\theta_1}{\theta_2}\right)^2 + \left(\frac{\theta_1\delta\theta_2}{\theta_2^2}\right)^2}, \quad (16)$$

where $\delta\theta_1$ and $\delta\theta_2$ are the errors propagated from $\delta\Delta\phi$ and $\delta\kappa$. The $\delta\theta$ is

$$(\delta\theta)^2 \simeq \left(1 + \frac{4}{5 + 3\cos 2\theta}\right)^2 \left[\left(\frac{\partial\theta_\mu}{\partial\Delta\phi}\right)^2 \delta\Delta\phi^2 + \left(\frac{\partial\theta_\mu}{\partial\kappa}\right)^2 \delta\kappa^2\right], \quad (17)$$

where

$$\frac{\partial\theta_\mu}{\partial\Delta\phi} = \frac{\sin\Delta\phi\ \sin\alpha\ \sin(\alpha+\beta)}{\sin\theta_\mu}, \quad (18)$$

$$\frac{\partial\theta_\mu}{\partial\kappa} = -\frac{[\sin\beta + 2\cos(\alpha+\beta)\ \sin\alpha\ \sin^2(\Delta\phi/2)]\beta}{\kappa\sin\theta_\mu}. \quad (19)$$

The errors for ζ can be derived in a similar fashion. We can also calculate numerical differentiations of the altitude ratio with respect to κ and $\Delta\phi$. Then we use the error propagation equation like Equation (16) to calculate the error induced from observational uncertainties $\delta\kappa$ and $\delta\Delta\phi$ in practical situation.

2.2. Applications to Selected Pulsar

Next we take PSR B0329+54, B1508+55, B2016+28, B1133+16, and B2319+60 as examples to show the quasi-independence of η, ζ. The κ values are adopted from Lyne & Manchester (1988) for all the pulsars. The pulse profile data for PSR B0329+54, B2016+28, B1133+16, and B2319+60 at 0.408 GHz and 1.4 GHz are from Gould & Lyne (1998). Except for PSR B1508+55, of which the 4.750 GHz data are from Seiradakis et al. (1995), all the other data at 4.85 GHz are from von Hoensbroech & Xilouris (1997). These pulsars are selected by the following criteria such that we can measure the intrinsic altitude ratio. (1) The interstellar scattering effect must be small so that the scattering affects little the measurement of $\Delta\phi$. (2) Pulse profile data have high signal-to-noise ratio to allow good measurement of $\Delta\phi$.

Assuming that the noise in and out of the pulse window are the same, the pulse profiles are fitted with a sum of Gaussians to measure the width of the pulse profile (Kramer et al. 1994; Wu et al. 1998, 2002; Qiao et al. 2003). The template to fit the pulse profile is

$$I(\phi, A_k, \phi_{c,k}, \sigma_k) = \sum_{k=1}^{n} A_k e^{-\ln 2\frac{(\phi-\phi_{c,k})^2}{\sigma_k^2}}, \quad (20)$$

where the number of Gaussians are n, I is the intensity of the pulse profile, A is the amplitude of each Gaussian component, ϕ_c is the center longitude of the Gaussian, and σ is the 50% intensity width of the Gaussian. The subscript "k" denotes the index of the Gaussians. The Levenberg–Marquardt method is used to search for $3n$ parameters $\{A_k, \phi_{c,k}, \sigma_k\}, k \in [1, n]$ to minimize the residue, Res, given as

$$\mathrm{Res} = \sum_{i=0}^{N} \left(I(\phi_i, A_k, \phi_{c,k}, \sigma_k) - I_i\right)^2, \quad (21)$$

where N is the number of data points of the pulse profile, $\{\phi_i, I_i\}$, $i \in [1, N]$, are observational data.

After fitting, the width of the pulse profile is estimated using

$$2\Delta\phi = \phi_{c,\mathrm{right}} - \phi_{c,\mathrm{left}} + 1.82262(\sigma_{\mathrm{right}} + \sigma_{\mathrm{left}}), \quad (22)$$

where $2\Delta\phi$ is the full width of the pulse profile measured down to 10% intensity, which is in concord with the standard notation (Kramer et al. 1994). The $\phi_{c,\mathrm{right}}$ and ϕ_{left} are the central longitude of the rightmost and the leftmost Gaussians, whose widths are σ_{right} and σ_{left}, respectively. The χ^2 test is adopted to estimate the error for $\Delta\phi$. The fitted pulse profiles for the five pulsars are given in Figure 8. The measured pulse width are listed in Table 2.

Using the method mentioned above, we calculate the relation between the inclination angle α and the altitude ratios (η and ζ) for the five pulsars, which are plotted in Figures 3–7. The values for $\frac{A_3}{A_1}$ are given in Table 3 and the values of the ratio η, ζ are given in Table 4. It is shown that the η and ζ are almost constants, when α changes from 0° to 90°. The variance of the ratio due to unknown α is smaller than the errors propagated from errors of κ and the pulse width. Thus, the ratios are insensitive to the unknown inclination angle α, which make the altitude ratio ζ be a better observational quantity than absolute radiation altitude.

In the next section, we will use the altitude ratios derived here to test the RS model and constrain the parameter space of the inverse Compton scattering model for radio pulsar.

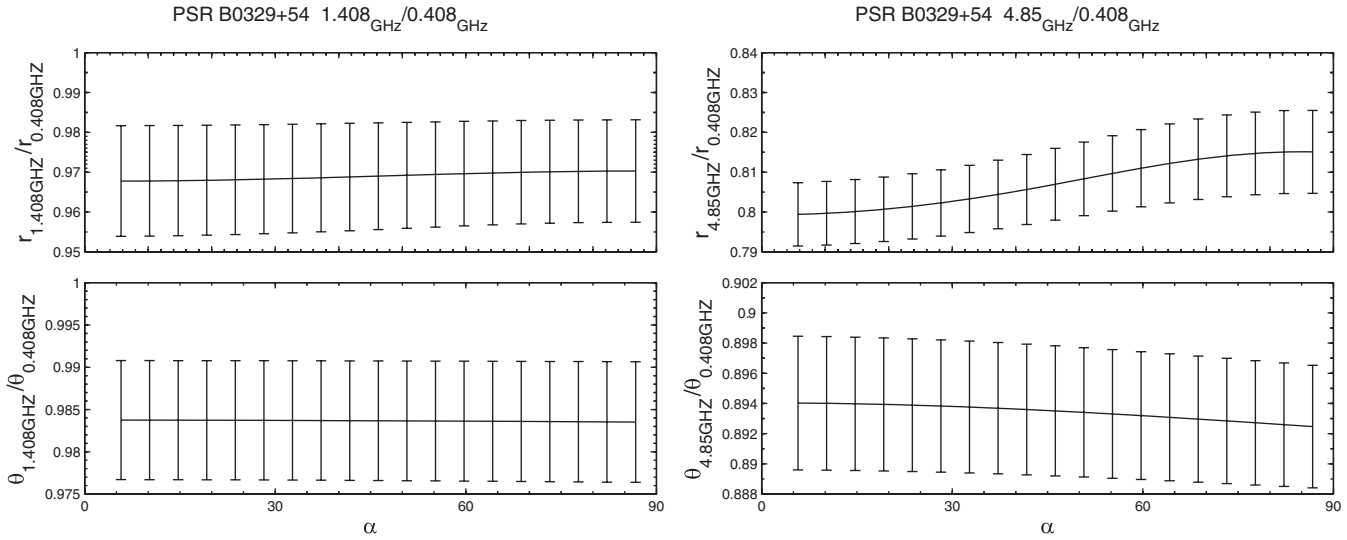

Figure 3. Radiation altitude ratios as functions of α for PSR B0329+54, where the subscript indicates the observing frequencies. The error bars indicate the error introduced by errors of $\Delta\phi$ and κ. It is clear that the error introduced by unknown α is smaller than the error passing from errors of $\Delta\phi$ and κ. Thus the ratios between different radiation altitudes are quasi-invariant for PSR B0329+54.

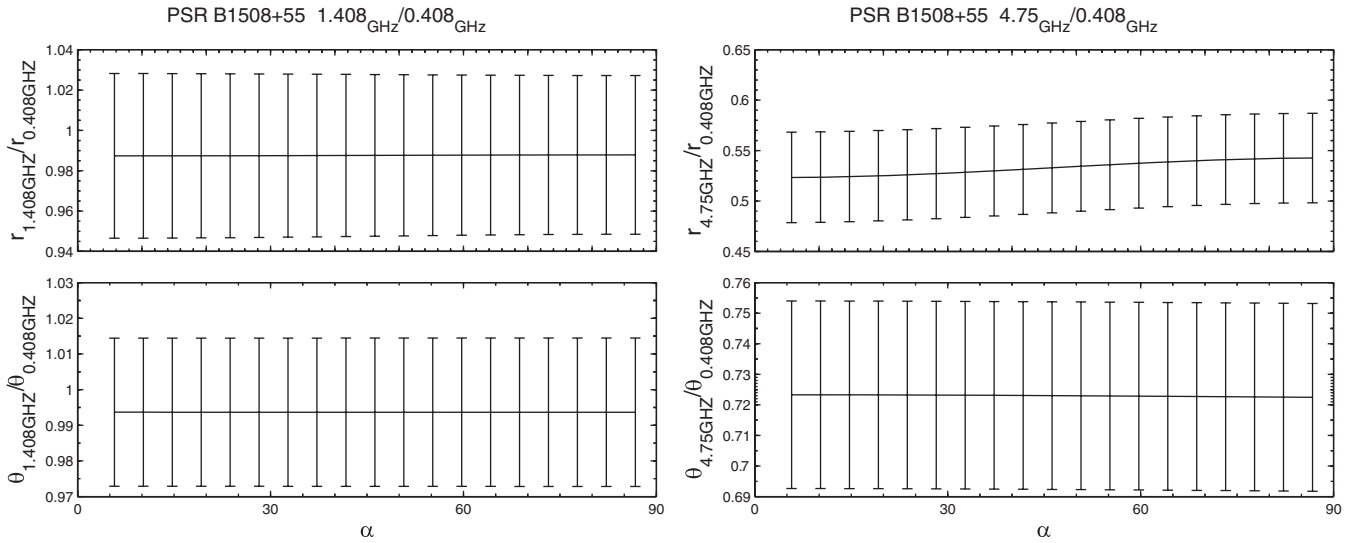

Figure 4. Radiation altitude ratios as functions of α for PSR B1508+55, where the subscript indicates the observing frequencies.

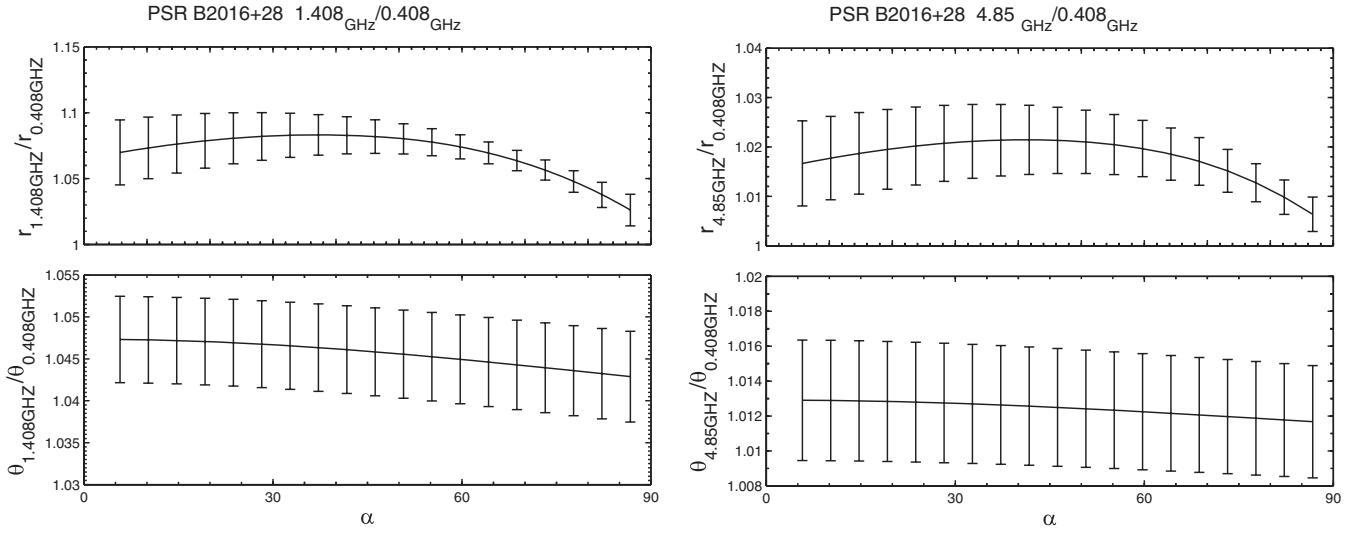

Figure 5. Radiation altitude ratios as functions of α for PSR B2016+28, where the subscript indicates the observing frequencies.

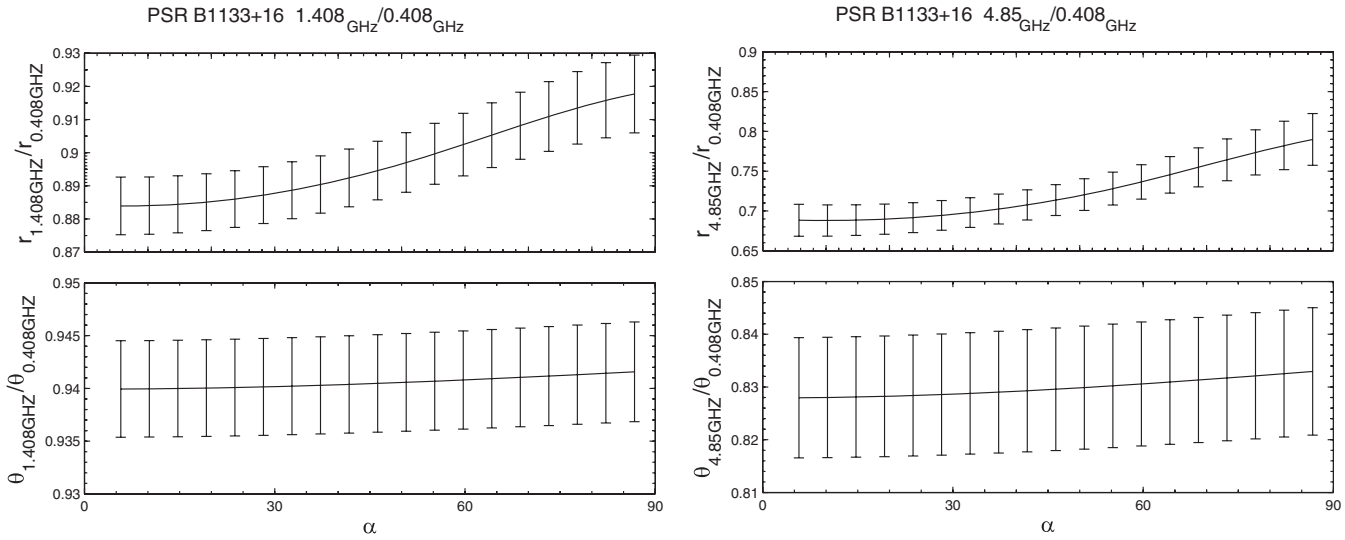

Figure 6. Radiation altitude ratios as functions of α for PSR B1133+16, where the subscript indicates the observing frequencies.

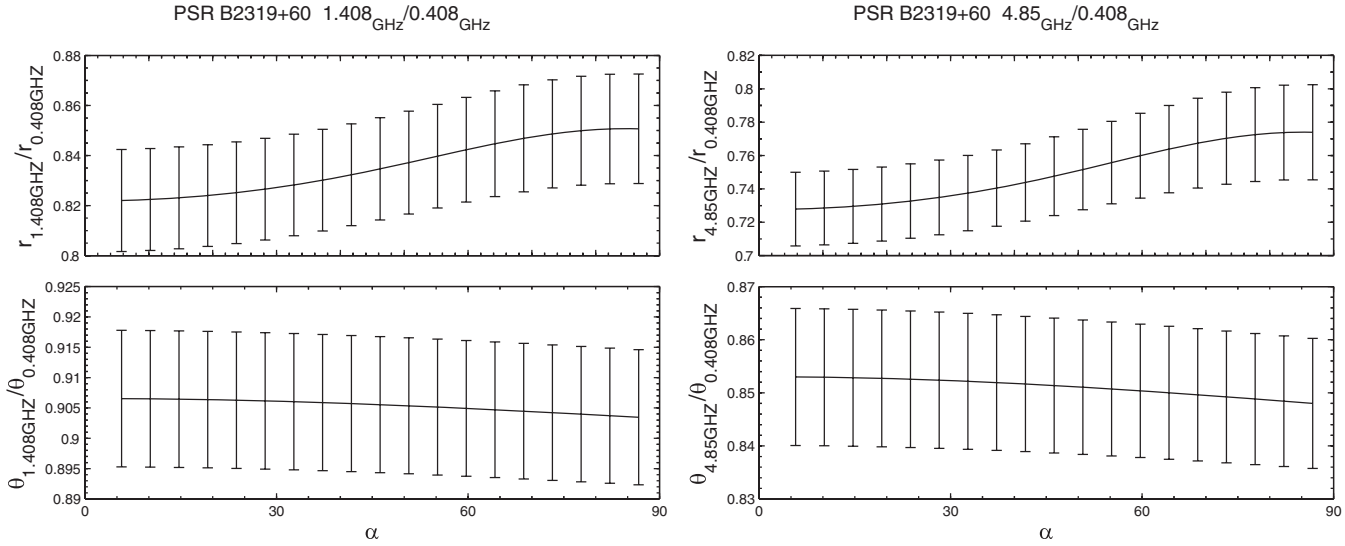

Figure 7. Radiation altitudes ratio as functions of α for PSR B2319+60, where the subscript indicates the observing frequencies.

Table 3
A_3/A_1 for PSR B0329+54, B1508+55, B2016+28, B1133+16, and B2319+60 at Multiple Frequencies

PSR	$\frac{A_3}{A_1}\|_{0.4\ \mathrm{GHz}}$	$\frac{A_3}{A_1}\|_{1.4\ \mathrm{GHz}}$	$\frac{A_3}{A_1}\|_{4.8\ \mathrm{GHz}}$	$\mathrm{Max}\left(\frac{A_3}{A_1}-\frac{A_3'}{A_1'}\right)$
PSR B0329+54	−0.1994	−0.2000	−0.2032	3.7×10^{-3}
PSR B1508+55	−0.2329	−0.2330	−0.2352	2.3×10^{-3}
PSR B2016+28	−0.2901	−0.2914	−0.2905	1.3×10^{-3}
PSR B1133+16	−0.2740	−0.2740	−0.2733	7.2×10^{-4}
PSR B2319+60	−0.2759	−0.2783	−0.2794	3.5×10^{-3}

Notes. The last column gives the maximal variance of A_3/A_1 among three frequencies. The difference between A_3/A_1 is on the order of 10^{-3}, thus the ratio will be insensitive with respect to α.

3. APPLICATIONS

3.1. Application for the RS Model

In this section, we apply the method to test the RS model. The RS model predicts that the radio wave with angular frequency ω coming from altitude r (Ruderman & Sutherland 1975) follows

$$r = 2\left(\frac{2\pi\gamma_{\max} eBR^3}{pm_e c}\right)^{1/3}\omega^{-2/3}, \tag{23}$$

where R is the pulsar radius, m_e is the rest mass of the electron, B is the surface magnetic field of the pulsar, $\gamma_{\max}$ is the maximal Lorentz factor of electrons. Assuming dipolar magnetic field, the polar angle for radiation location will be $\theta \simeq \sqrt{r/R_{\rm LC}}$. Thus,

$$\theta = 4.5\times10^{-2}\, p^{-7/12}\,\dot{p}_{[-15]}^{1/12}\gamma_{\max}^{1/6}\,\omega_{\rm GHz}^{-1/3}, \tag{24}$$

where $\omega_{\rm GHz}$ is the angular frequency of radio wave in unit of GHz, $\dot{p}_{[-15]}$ is the period derivative in unit of 10^{-15} s/s, period p is in unit of second. The radiation altitude ratio by the RS model is then

$$\frac{\theta_1}{\theta_2} = \left(\frac{\omega_2}{\omega_1}\right)^{1/3}, \tag{25}$$

$$\frac{r_1}{r_2} = \left(\frac{\omega_2}{\omega_1}\right)^{2/3}. \tag{26}$$

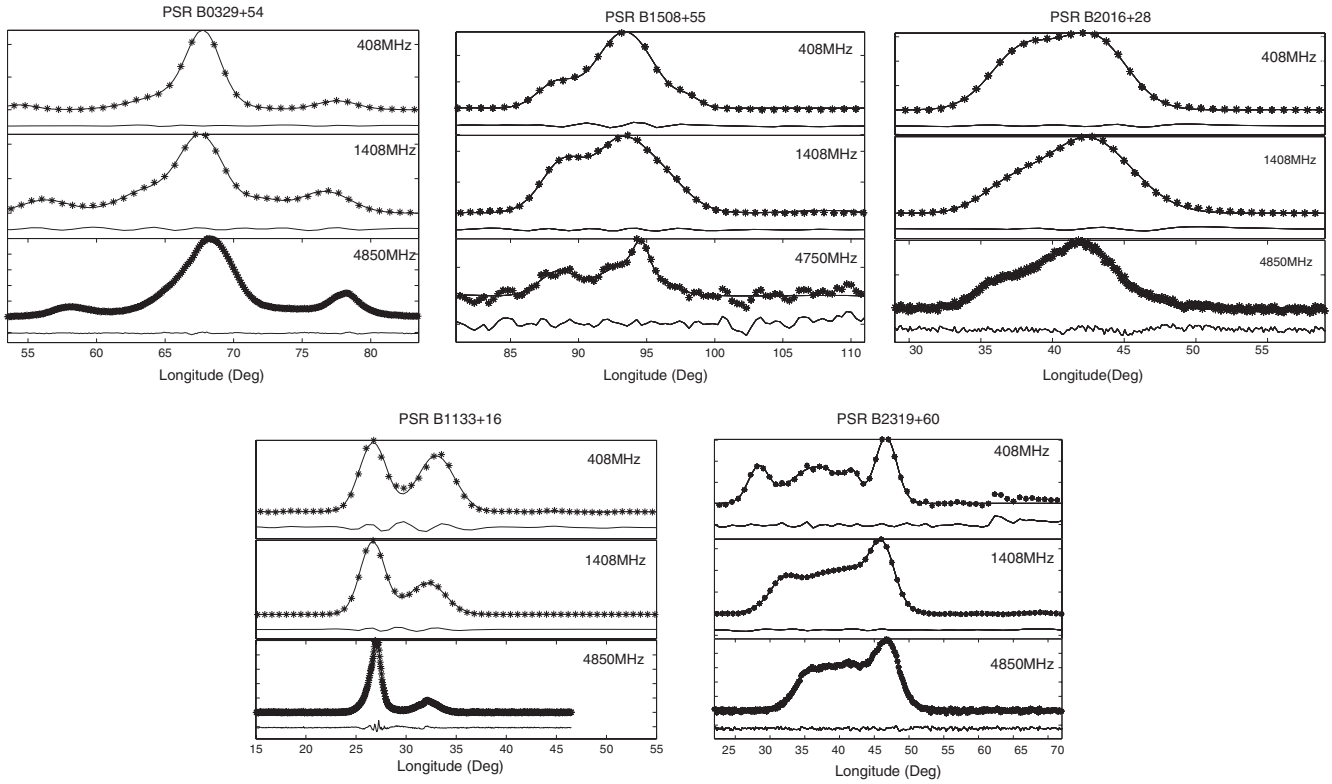

Figure 8. Observed pulse profile data, fitted pulse profile, and fitting residue for B0329+54, B1508+55, B2016+28, B1133+16, and B2319+60. The "*" symbol corresponds to the observed pulse profile, the fitted pulse profile is indicated by the solid line, and the fitting residual is plotted in the lower panel.

In this way the RS model predicts $\theta_{1.4\,\mathrm{GHz}}/\theta_{0.408\,\mathrm{GHz}} = 0.70$ and $\theta_{4.8\,\mathrm{GHz}}/\theta_{0.408\,\mathrm{GHz}} = 0.46$ for all pulsars. This is clearly incomparable with the ratio we measured in the previous section. Thus, the RS model needs improvement in order to explain the observed RFM.

3.2. Application for the ICS Model

In this section, we use the method developed in Section 2 and the radiation altitude ratios of PSR B2016+28 and PSR B0950+08 to constrain the parameter space of the ICS model.

The ICS model proposed that low-frequency radio waves are produced in polar gap sparking and then are inverse Compton scattered by high-energy secondary particles to form the observed radio radiation beams (Qiao & Lin 1998). One prediction of the model is that the radio waves of different frequencies come from different altitudes (see the "beam-frequency figures" in Qiao et al. 2001 for details).

The ICS model proposes that low-frequency radio wave with frequency ω_0 is produced by polar gap sparking, and then inverse Compton scattered by secondary particles, of which the Lorentz factor is γ, to a higher frequency $\omega' = 2\gamma^2\omega_0(1 - v\cos\theta_i/c)$, where v is the velocity of secondaries. We take $v/c = 1$ because the velocity of secondaries is ultra relativistic (γ is about several hundred). The θ_i is the angle between the direction of propagation of low-frequency radio wave and the direction of velocity of secondaries, which satisfies (Qiao et al. 2001)

$$\cos\theta_i = \frac{2\cos\theta - (R/r)(1 - 3\cos^2\theta)}{\sqrt{(1 + 3\cos^2\theta)[1 - 2(R/r)\cos\theta + (R/r)^2}}, \quad (27)$$

the ICS model assumes that the Lorentz factor γ of secondaries will reduce due to energy loss, which follows $\gamma = \gamma_0[1 - \xi(r - R)/R_e]$, where γ_0 and ξ are the initial Lorentz factor for secondaries and the energy loss factor, respectively. γ_0, ξ, and ω_0 are three total parameters for the ICS model. In this paper, we constrain the parameter space for γ_0 and ξ, while fix $\omega_0 = 10^6$ Hz following the conventional assumption of the ICS model. In fact, because ω_0 is always multiplied with γ_0^2, the degrees of freedom for ω_0 and γ_0 are degenerated. Thus, we can fix $\omega_0 = 10^6$ Hz without losing generality.

Using the above equations, we calculate the ratio between radiation altitudes of different frequencies as a function of α using the ICS model. Then we compared the simulated ratios with the ratio measured using the method given in Section 2 to constrain the range of parameters γ_0 and ξ. The results for the five pulsars are presented in Figure 9. To meet the observations, the initial Lorentz factor for the ICS model should be of the order of 10^3–10^4.

4. CONCLUSION AND DISCUSSION

We have presented an algorithm for calculating the ratio between the radiation altitudes of pulsars observed at different frequencies, given multifrequency pulse profiles and linear polarization position angle curve. It is shown that the ratio between emission altitudes will be insensitive to the inclination angle α, if the polarization position angle curves are steep, i.e., $\kappa \gg 1$. This algorithm offers us a method to determine the relative radiation altitudes to a high accuracy.

Because the selected pulsar examples have long enough period (order of 10^{-1} to 1 s) compared to the pulse broadening due to scattering (order of 1 ms estimated from the dispersion measure), we have ignored the scattering effects when determining the pulse width (Mitra & Ramachandran 2001). Scattering effects introduce less than 1° error in measuring the pulse width (Li & Han 2003). Rankin (1983, 1990) pointed out that the pulse morphology is rather complex. In this paper, we

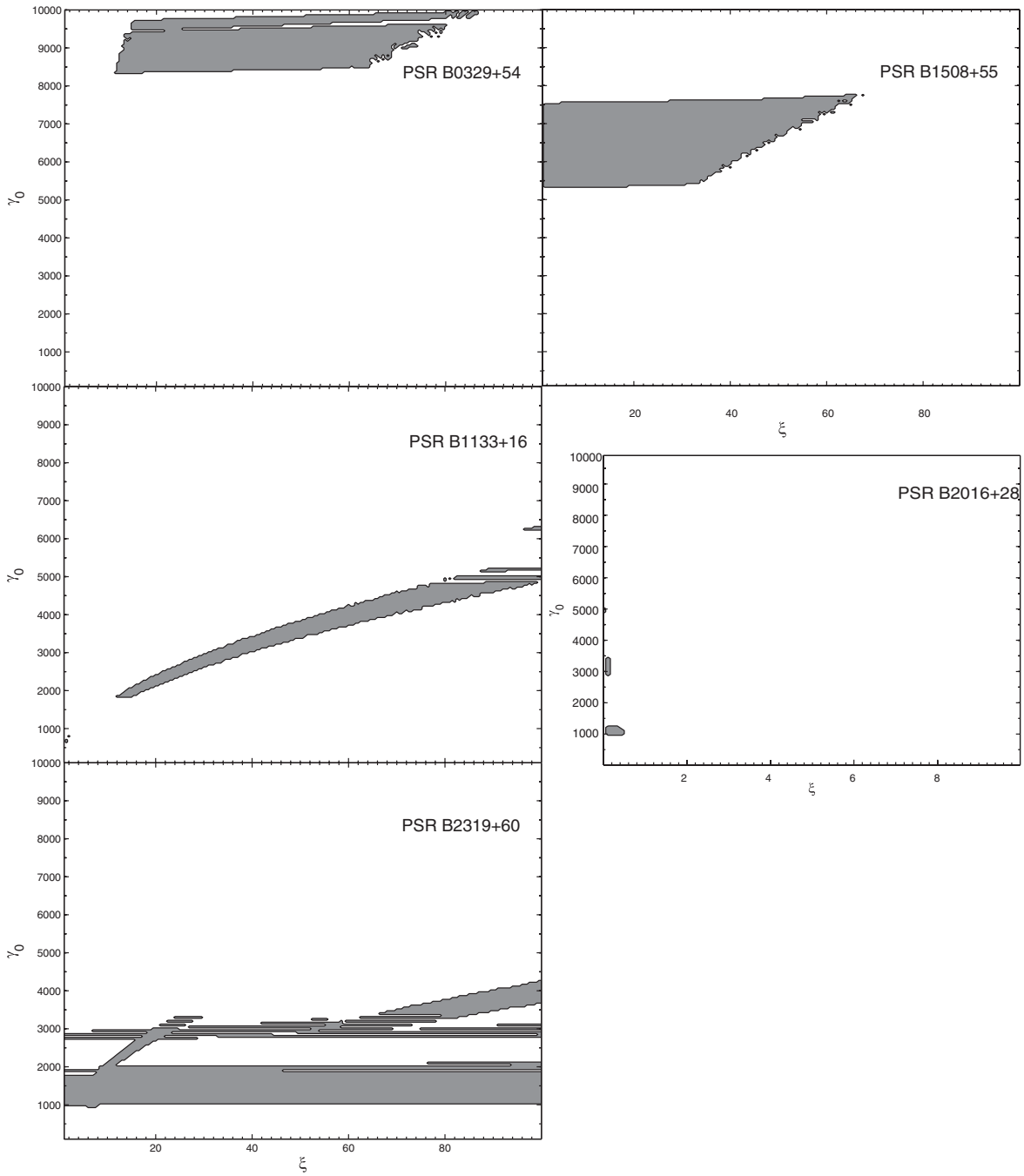

Figure 9. Allowable parameter space of the ICS model for PSR B0329+54, B1508+55, B2016+28, B1133+16, and B2319+60. γ_0 and ξ are the initial Lorentz factor for secondaries and energy loss factor for the ICS model. The gray areas are the possible parameter space for the ICS model that give radiation altitude ratio compatible with our measurements. The branching behavior of the gray area is due to the property of the ICS model, in which radio wave with the same frequency comes from up to three different altitudes. Note that the panels for PSR B2016+28 have different scales.

use the total pulse width, within which the dominate part of the radiation beam is included. Thus, we do not perform the pulse-profile-component identification such as that in Srostlik & Rankin (2005b).

Because we use only the pulse width of the pulse profile rather than the relative phase shift, we ignore the effects of magnetic field line bending, aberration, and retardation. The magnetic field line bending and aberration will be second order effects for our method, although they are first order effects for phase shift of pulse components (Phillips 1992; Gangadhara 2005; Lee et al. 2006).

Although the altitude ratio is insensitive to the inclination angle, the absolute altitudes are sensitive to the inclination angle. In this way, our three-dimensional method does not measure absolute altitudes solely. However, when combining with radiation altitude measured at one frequency, we can easily calculate the altitudes for other frequencies.

There is no last open magnetic field line assumption in calculating η. However, we have assumed that the radiation comes from last open magnetic field lines, when calculating ζ. This assumption can be weakened for radiation coming from

Table 4
Measured Value of η and ζ for PSR B0329+54, B1508+55, B2016+28, B1133+16, and B2319+60

PSR	1.4 GHz/0.408 GHz	4.8 GHz/0.408 GHz
PSR B0329+54		
η	0.98 ± 0.01	0.89 ± 0.01
ζ	0.97 ± 0.02	0.81 ± 0.02
PSR B1508+55		
η	0.99 ± 0.02	0.72 ± 0.03
ζ	0.99 ± 0.04	0.53 ± 0.05
PSR B2016+28		
η	1.05 ± 0.01	1.01 ± 0.004
ζ	1.07 ± 0.04	1.02 ± 0.01
PSR B1133+16		
η	0.94 ± 0.01	0.83 ± 0.01
ζ	0.90 ± 0.03	0.72 ± 0.08
PSR B2319+60		
η	0.91 ± 0.01	0.85 ± 0.02
ζ	0.84 ± 0.04	0.75 ± 0.05

Notes. η is the ratio between polar angles of radiation locations, i.e., $\eta = \theta_1/\theta_2$. ζ is the ratio between altitudes of radiation locations, i.e., $\zeta = r_1/r_2$. Here, the errors in this table include both the error from the tiny dependence of ratio on the inclination angle and the error induced from the errors of κ and $\Delta\phi$.

magnetic field lines with same R_e. If so, the R_e can be canceled in calculating the ratio ζ.

Using the accurately measured radiation altitude ratios, we can test or constrain the parameter space for pulsar radiation models. We take the RS model and the inverse Compton scattering model as examples to show the application of this technique. For the RS model, our analysis show inconsistency between the RS model prediction and observed radiation altitude ratios. This may be due to the rough treatments of secondaries' energy loss and rough estimation for the RFM in the RS model or due to the incorrect radiation scenario (i.e., whether the radio radiation is really generated through the curvature radiation). For the ICS model, our results are consistent with the results of Zhang et al. (2007). The parameter space of PSR B2016+28 is limited to a smaller region due to smaller error of the measured ratio compared to others. It should be easy to generalize this method to other radiation models, which predicted the relation between the radiation altitude and the radiation frequency.

Because we do not use the relative time delay of radiation components, our method will be easily generalized to high energy band without dispersion delay correction. Thus, this method will also be good tool to study high energy radiation processes, such as radiation processes in γ-ray bands and X-ray bands. The ongoing project FERMI will provide a higher quality γ-ray data, which will be an ideal target to study the pulsar radiation mechanism using this method.

It has been realized that there is inconsistency in measuring the altitudes between using time delay methods and using geometrical methods (Mitra & Li 2004). Our method will be affected neither by propagation effects nor by unknown inclination angle. Thus, the method could offer a check for the present absolute altitude measurements.

This method will also be a tool for pulsar timing researches. Pulsar timing is now pushing the limit to the accuracy of about 100 ns (van Straten et al. 2001). To achieve such accuracy, the altitudes of radiation should not change more than 30 m. Because our method of determining the altitude ratio of radiation location can, in principle, achieve accuracy of 10^{-4}, we could study the effects of pulsar timing noise induced by radiation altitude variation.

We are grateful to the anonymous referee for very helpful constructive suggestions and help on choosing pulsar sources. We are also grateful to J. L. Han, R. T. Gangadhara, and C. K. Chou for discussions and comments. This work was supported by NSFC (10833003, 10778611) and the National Basic Research Program of China (grant 2009CB824800).

APPENDIX

PULSAR RADIATION GEOMETRY

In this appendix, we derive the analytic form equations for pulsar radiation geometry. More details and discussions about the high-order effects, such as aberration, retardation, and relativistic light bending, can be found in Lee (2003).

We call the Cartesian coordinate O–$X'Y'Z'$ magnetic coordinate and the Cartesian coordinate O–XYZ lab coordinate, where the Z-axis of the lab coordinate is the rotation axis of the pulsar; and the Z'-axis of the magnetic coordinate is the magnetic axis of the pulsar. We choose the coordinates such that we align the Y- and Y'-axes. These two coordinates are just generated by angular rotation about the Y-axis with angle α with respect to each other. The coordinate transformation between two coordinates is given by

$$\begin{pmatrix} x \\ y \\ z \end{pmatrix} = \begin{pmatrix} \cos\alpha & 0 & \sin\alpha \\ 0 & 1 & 0 \\ -\sin\alpha & 0 & \cos\alpha \end{pmatrix} \begin{pmatrix} x' \\ y' \\ z' \end{pmatrix}, \tag{A1}$$

where symbols with $'$ denote the coordinates value in the magnetic coordinate and α is the inclination angle. The coordinate values for magnetic field lines ($r = R_e \sin^2\theta$) in the magnetic coordinate are

$$\begin{pmatrix} x' \\ y' \\ z' \end{pmatrix} = R_e \begin{pmatrix} \sin^3\theta\,\cos\varphi \\ \sin^3\theta\,\sin\varphi \\ \sin^2\theta\,\cos\theta \end{pmatrix}. \tag{A2}$$

So, the coordinates of magnetic field lines in the lab coordinate are

$$\begin{pmatrix} x \\ y \\ z \end{pmatrix} = R_e \begin{pmatrix} \sin^2\theta(\cos\alpha\cos\varphi\sin\theta + \cos\theta\sin\alpha) \\ \sin^3\theta\sin\varphi \\ \sin^2\theta(\cos\alpha\cos\theta - \cos\varphi\sin\alpha\sin\theta) \end{pmatrix}. \tag{A3}$$

The half width of the beam angle θ_μ can be calculated in the magnetic coordinate. We have

$$\tan\theta_\mu = \left.\frac{\partial_\theta x'}{\partial_\theta z'}\right|_{\varphi=0} = \frac{3\sin 2\theta}{3\cos 2\theta + 1}. \tag{A4}$$

Thus, the radiation beam projected onto the unit sphere in the lab coordinate is

$$\begin{pmatrix} x_{\rm beam} \\ y_{\rm beam} \\ z_{\rm beam} \end{pmatrix} = \begin{pmatrix} \cos\theta_\mu\sin\alpha + \cos\alpha\cos\varphi\sin\theta_\mu \\ \sin\theta_\mu\sin\varphi \\ \cos\alpha\cos\theta_\mu - \cos\varphi\sin\alpha\sin\theta_\mu \end{pmatrix}. \tag{A5}$$

Given the observer with impact angle β. The two observable points for the radiation beam satisfy $z_{\rm beam} = \cos(\alpha + \beta)$, which is just (Equation (5))

$$\cos\alpha\cos\theta_\mu - \cos\varphi\sin\alpha\sin\theta_\mu = \cos(\alpha + \beta). \tag{A6}$$

Putting Equation (A6) into Equation (A5), we can get the x-components of the coordinate for the radiation beam

$$x_{\rm beam} = \cos\theta_\mu\csc\alpha - \cos(\alpha + \beta)\cot\alpha. \tag{A7}$$

Note that $z_{\rm beam} = \cos(\alpha+\beta)$, we have following equation for the half angular width $\Delta\phi$ for the pulse of pulsar:

$$\cos\Delta\phi = \frac{x_{\rm beam}}{\sin(\alpha+\beta)} = \frac{\cos\theta_\mu - \cos(\alpha+\beta)\cos\alpha}{\sin\alpha\sin(\alpha+\beta)}, \quad \text{(A8)}$$

which could be easily converted to Equation (2) (Lyne & Manchester 1988).

For Equation (A3), we can calculate the length $l = \sqrt{x^2+y^2}$ of a point on magnetic field lines to the rotation axis. The last open magnetic field lines are tangent to the light cylinder, so we have

$$R_{\rm LC} = R_{\rm e}\sin^2\theta_{\rm M}\sqrt{1-(\cos\alpha\cos\theta_{\rm M} - \cos\varphi\sin\alpha\sin\theta_{\rm M})^2}. \quad \text{(A9)}$$

It is clear that the l reaches its maximal value at $\theta_{\rm M}$, thus we have (in fact this is Equation (7))

$$\left.\frac{\partial l}{\partial\theta}\right|_{\theta=\theta_{\rm M}} = 0. \quad \text{(A10)}$$

REFERENCES

Blaskiewicz, M., Cordes, J. M., & Wasserman, I. 1991, ApJ, 370, 643
Cordes, J. M. 1978, ApJ, 222, 1006
Gangadhara, R. T. 2005, ApJ, 628, 923
Gangadhara, R. T., & Gupta, Y. 2001, ApJ, 555, 31
Gil, J., Gronkowski, P., & Rudnicki, W. 1984, A&A, 132, 312
Gil, J. A., & Kijak, J. 1993, A&A, 273, 563
Gould, D., & Lyne, A. 1998, MNRAS, 301, 225
Johnston, S., Kramer, M., Karastergiou, A., Hobbs, G., Ord, S., & Wallman, J. 2007, MNRAS, 381, 1625
Kijak, J., & Gil, J. 1997, MNRAS, 288, 631
Kijak, J., & Gil, J. 2003, A&A, 397, 969
Kramer, M., Wielebinski, R., Jessner, A., Gil, J. A., & Seiradakis, J. H. 1994, A&AS, 107, 515
Lee, K. J. 2003, Bachelor thesis, Peking Univ.
Lee, K. J., Qiao, G. J., Wang, H. G., & Xu, R. X. 2006, Adv. Space Res., 37, 1988
Li, X. H., & Han, J. L 2003, A&A, 410, 253
Lyne, A. G., & Manchester, R. N. 1988, MNRAS, 234, 477
Mitra, D., & Li, X. H. 2004, A&A, 421, 215
Mitra, D., & Ramachandran, R. 2001, A&A, 370, 586
Phillips, J. A. 1992, ApJ, 385, 282
Qiao, G. 1988, Vistas Astron., 31, 393
Qiao, G. J., Li, K. J., Wang, H. G., Xu, R. X., & Liu, J. F. 2003, Acta Astron. Sin., 44, 230
Qiao, G. J., & Lin, W. P. 1998, A&A, 333, 172
Qiao, G. J., Liu, J. F., Zhang, B., & Han, J. L. 2001, A&A, 377, 964
Radhakrishnan, V., & Cooke, D. J. 1969, Astrophys. Lett., 3, 225
Rankin, J. M. 1983, ApJ, 274, 333
Rankin, J. M. 1990, ApJ, 352, 247
Ruderman, M. A., & Sutherland, P. G. 1975, ApJ, 196, 51
Seiradakis, J. H., Gil, J. A., Graham, D. A., Jessner, A., Kramer, M., Malofeev, V. M., Sieber, W., & Wielebinski, R. 1995, A&AS, 111, 205
Srostlik, Z., & Rankin, J. M. 2005a, MNRAS, 362, 1121
Srostlik, Z., & Rankin, J. M. 2005b, MNRAS, 362, 1121
van Straten, W., Bailes, M., Britton, M., Kulkarni, S. R., Anderson, S. B., Manchester, R. N., & Sarkissian, J. 2001, Nature, 412, 158
von Hoensbroech, A., & Xilouris, K. M. 1997, A&AS, 126, 121
Wang, H. G., Qiao, G. J., Xu, R. X., & Liu, Y. 2006, MNRAS, 366, 945
Wu, X., Gao, X., Rankin, J. M., Xu, W., & Malofeev, V. M. 1998, AJ, 116, 1984
Wu, X.-J., Huang, Z.-K., & Xu, X.-B. 2002, Chin. J. Astron. Astrophys., 2, 454
Xu, R. X., Liu, J. F., Han, J. L., & Qiao, G. J. 2000, ApJ, 535, 354
Zhang, H., Qiao, G. J., Han, J. L., Lee, K. J., & Wang, H. G. 2007, A&A, 465, 525